Master de Sciences de la Terre et de la Planète, Géodynamique et Géomatériaux.
2024/2025

Characterisation and modeling of saline intrusions in the plain of Roussillon.

Santa KAMUTI
Master 1

MENTORS:
Delphine ROUBINET
Laurent BRUN
Johanna LOFI

Defended on the 20th of July 2025 before the jury members:
Andrea TOMMASI (Reviewer)
Benoit GIBERT (Reviewer)
Alfredo TABOADA
Jean-Roch PALASSE
Frédéric GUEYDAN

Contents

Characterisation and modeling of saline intrusions in the plain of Roussillon.

Abstract

This study investigates salt water intrusion in the multilayered coastal aquifer systems of the Roussillon Plain, considering both natural and anthropogenic influences on groundwater dynamics. Using data from previous projects - SWIMCLAS and Dem'Eaux- we characterise saltwater through geophysical methods, notably Nuclear Magnetic Resonance (NMR) and petrophysical analysis, which inform us on lithological characterisation and water detection. These data will support our numerical model developed in MODFLOW, with a focus on simulating coupled transport of fluids and solutes under density-dependent flow conditions. A conceptual three layer (clay-sand-clay) system, representing our study zone- the Demmer 4 well area- is used to explore the effects of key hydrogeological parameters on saline intrusions. The critical parameters include hydraulic conductivity, porosity, and permeability, which we varied to evaluate their impact on the saline intrusion. We simulate steady state, 2D freshwater flow into a confined aquifer, and analyze the evolution of the resulting mixing zone. Results reveal a pronounced wedge-shaped saline interface, with intrusion depth strongly dependent on permeability contrasts. This approach contributes to comprehending the mechanisms of saltwater encroachment in coastal aquifers.

Résumé

Cette étude examine l'intrusion saline au sein des systèmes aquifères côtiers multicouches de la plaine de Roussillon, en intégrant à la fois les influences naturelles et anthropiques sur la dynamique des eaux souterraines. A partir des données issues des projets précédents- SWIMCLAS et Dem'Eaux- nous caractérisons l'intrusion saline en s'appuyant sur les méthodes géophysiques, notamment la Résonance Magnétique Nucléaire (RMN) et les analyses pétrophysiques, utilisées pour nous informer sur la caractérisation lithologique et la détection de l'eau. Ces données alimentent notre modèle numérique développé sous MODFLOW, mettant l'accent sur le transport couplé des fluides et des solutés dans des conditions d'écoulement dépendant de la densité. Un modèle conceptuel d'un aquifère à trois couches alternées (argile–sable–argile), associé à un puit hypothétique (représentant notre zone d'étude autour du puit Demmer 4), est utilisé pour explorer les effets de paramètres hydrogéologiques clés sur l'intrusion saline. Les paramètres critiques, tels que la conductivité hydraulique, la porosité et la perméabilité, sont modifiés pour évaluer leur influence sur l'intrusion saline. Nous simulons un écoulement d'eau douce en régime permanent en 2D dans un aquifère captif, et analysons l'évolution de la zone de mélange résultante. Les résultats révèlent une interface saline marquée en forme de "wedge", dont la profondeur d'intrusion dépend fortement des contrastes de perméabilité. Cette approche numérique améliore notre compréhension des mécanismes d'intrusion saline dans les aquifères côtiers.

Key words: Roussillon aquifer, Saltwater intrusion, Variable Density Flow (VDF), Sea water intrusion (SWI), Coastal aquifers (CAs), Numerical modeling.

1. Introduction

Coastal aquifers play a crucial role in the supply of potable water and agricultural irrigation in multiple mediterranean regions. In the Roussillon plain, the pressure exerted on the water resources has intensified during the last decades, due to population growth, seasonal tourism, and climate change, which manifests itself by a decrease in rainfall and sea level rise. This pressure has led to a significant decline in the piezometric level in the water tables, creating conditions conducive to potential saline intrusion. SWI leads to progressive degradation of the underground water quality, with severe consequences for agriculture and potable water. The phenomenon is accentuated by excessive pumping, especially during summer seasons with hotter and drier temperatures, and the natural fluctuations or the anthropogenic influences on water levels *(Caballero et al., 2020)*.

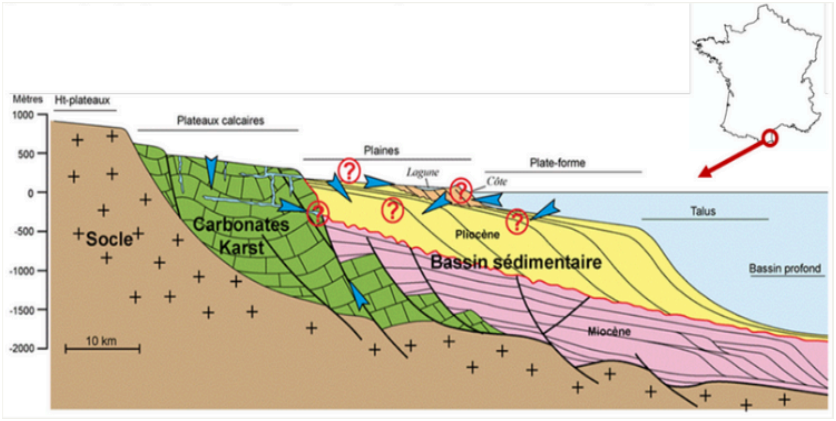

Fig. 1. Geological cross section of the Roussillon plain (Duvail and Aunay, 2005).

The Plio-Quaternary aquifer of Roussillon contains a multilayer alluvial formation, with levels of sand from the Quaternary and clay from the Pliocene, stacked over a thickness of up to 300m. These alluvial deposits extend beneath the Mediterranean Sea, integrating into the continental platform of the Gulf of Lion. The groundwater resource found in these formations is heavily exploited near the surface and is susceptible to discharge beneath the sea, through exact distances and depths that remain unknown *(Caballero et al., 2020)*.

Vertical drainage fluxes as of today are oriented from the Quaternary towards the Pliocene due to the intense pumping of Pliocene aquifers; it demonstrates an inversion of the natural flow direction that existed prior to groundwater extraction *(Caballero et al., 2020)*. This induced downward drainage creates a risk of deep contamination by either diffuse pollutants (such as nitrates and pesticides) or saltwater, both of which circulate within the Quaternary formations onshore and near the coastline *(Caballero et al., 2020)*. Interpretations of pumping tests show that groundwater flow within the Pliocene is strongly controlled by the geometry of sandy deposits, with drawdowns that can laterally extend over distances of several kilometers. It can be concluded that outcropping Pliocene formations benefit from recharge by precipitation and rivers draining the surrounding massifs, such as the Corbière's massif, as well as from contributions from the overlying Quaternary formations. The magnitude of these vertical fluxes is largely controlled by the intensity of pumping in the Pliocene aquifer.

Numerous projects have led to better understanding of this phenomenon. One such project, **SWIMCLAS**, was conducted as a second year master's internship and aimed to advance knowledge by integrating geology, hydraulics and modelling. It demonstrates that it is possible to

mitigate SWI with increased inflow, which represents the natural ambient water flow in our aquifer system. Another initiative, the **Dem'Eaux** project, led by the BRGM and implemented from 2017 up until 2022, reunited geologists, geochemists, geophysicists, among others to categorize the interactions of coastal aquifers with climate, surface water and the sea. Their interest lies in new management methods and the surveillance for aquifers in the Roussillon sedimentary basin. This project was developed in 2023–2024 as part of the SwimClas project, funded by the UNESCO-ICERWARD center. The project enabled the execution of NMR measurement campaigns and the supervision of a Master 2 thesis. Since 2024, the continuation of this research has been supported through the ANR AQUIMER project. The project is carried out in collaboration with Geosciences Montpellier, BRGM, and other scientific partners. The **objective** of this internship is to analyse information from various sources and formats in order to gain a deeper understanding of the evolution of Saltwater Intrusion (SWI) in coastal aquifers (CAs). To achieve this, several key tasks were planned.

First, **data processing** which involved reviewing and analysing existing datasets. Petrophysical data obtained from borehole cores and geophysical well logs provide a comprehensive basis for characterization of the lithology and the estimation of key properties such as porosity and permeability. Porosity was estimated from travel time*(Timur, 1968)* and permeability was thereafter derived as a function of porosity *(Timur, 1968, Coates et al., 1999)*. The empirical relationship between them provides essential inputs for understanding the flow capacity of the aquifer materials. Second, **hydrogeological modeling which** was carried out using MODFLOW software to simulate SWI processes under varying conditions**.** Building on the processed petrophysical data, we simulate dynamic behaviour of fluid flow and solute transport within our porous media using a variable-density flow (VDF) model. This model couples **Darcy's law** with **advection–dispersion equations**, incorporating **Fick's law** to account for molecular diffusion *(Bear., 1972*). This approach captures the complex interactions between saltwater and freshwater in CAs, allowing for realistic simulation of density-driven flow and salinity transport.

In this report, we present the context and review relevant literature underpinning our study. We outline the methodological approaches developed and refined throughout the research. Finally, we discuss preliminary results, which will be further expanded upon and analysed upon until the conclusion of the internship at the end of August.

2. Literature review

This section provides a comprehensive review of data types and scientific articles relevant to the study. The review focuses on saltwater intrusion processes, Nuclear Magnetic Resonance (NMR) techniques and, petrophysical data analysis. Additionally, we review the fundamental equations governing VDF, which form the basis of the modelling approaches used in this study.

2.1 Nuclear Magnetic resonance.

Nuclear Magnetic Resonance (NMR) allows direct detection of groundwater, in addition to providing information about groundwater distribution and the mean size of the pores of water-saturated rocks (*Meju et al., 2002*). The physical phenomenon behind the NMR log is the response of hydrogen nuclei to a magnetic field, by means of its magnetic moment. This moment, which reflects the capacity of hydrogen nuclei to align with the induced magnetic field, depends on the nuclei excitation which occurs at a specific resonance frequency known as the Larmor frequency *(Coates et al., 1999)*. When the nuclei return to their initial state, they emit a precession

signal that induces a magnetic field and can thus be detected *(Fig.2.)*. The shape of this signal depends on the speed at which the nuclei return to their initial state. In a porous medium, different types of signals will be observed depending on the distribution of water within the pore space. *(Legchenko., 2002)*.

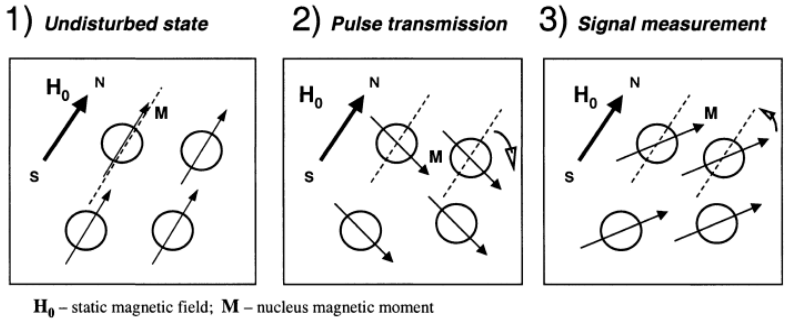

Fig. 2. The different phases of magnetic resonance (Legchenko., 2002).

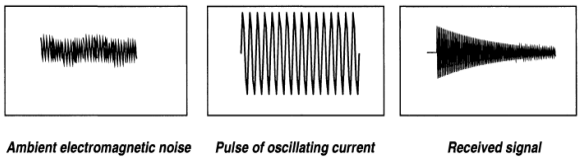

Fig. 3. Measurements of corresponding magnetic resonance. (Polarization > Excitation > Detection) (Legchenko., 2002).

2.2 Variable Density Flow

Variable Density Flow (VDF) is described by the variable-density groundwater flow equation *(Langevin et al., 2008)*. In models that incorporate VDF, the fluid density depends on the salt concentration *(Koohbora, 2019)*. This relationship is typically expressed through an equation of state for the fluid mixture. VDF models involve coupled flow and mass transport equations. The flow equation (Darcy's Law)(1) and the mass transport equation (advection-dispersion equation for solute concentration) are interdependent, as the fluid density in the flow equation is influenced by the concentration computed in the mass transport equation *(Mozafari, 2018)*. These models enable the simulation of groundwater flow while accounting for the transport of dissolved salt.

$$Q = -KA\frac{\Delta h}{L} \quad (1)$$

Where Q is the flow rate (m^3/day), K is hydraulic conductivity(m/s),
$A\frac{\Delta h}{L}(m/m)$ *is the hydraulic gradient, h is the hydraulic head(m)*
and L is the distance travelled(m).

The variable density state flow is defined by the following equation *(Langevin et al., 2008)*.

$$\nabla.\left[\rho\frac{\mu_0}{\mu}K_0\left(\nabla h_0 + \frac{\rho-\rho_0}{\rho_0}\nabla z\right)\right] = \rho S_{s,0}\frac{\partial h0}{\partial t} + \theta\frac{\partial \rho}{\partial t}\frac{\partial C}{\partial t} - \rho_s q'_s, \quad (2)$$

Flow equation takes into consideration density, viscosity, porosity, hydraulic head, salt concentration, and the volume of water released into the aquifer.

2.3 The Henry Problem

The **Henry problem** is a classical benchmark for studying Saltwater intrusion (SWI) in Coastal aquifers (CAs). It represents a simplified two-dimensional vertical cross-section of a confined aquifer with homogeneous, isotropic hydraulic conductivity, perpendicular to the coastline *(Fig. 4.)*. The model assumes VDF and considers both advection and diffusion, but neglects dispersion *(Mozafari., 2018)*. The model postulates a homogeneous aquifer with fixed limits: a salt concentration of 35g/l and a hydraulic head of 0 is applied on the seaward side, and an influx of freshwater on the inland side. Software environments such as COMSOL Multiphysics are used to implement VDF models by coupling groundwater flow modules based on Darcy's law with dilute species transport modules, assuming fluid density is concentration-dependent *(Mozafari, 2018, Koohbora, 2019)*. Discrete Fractured Networks (DFN) models can be integrated within the VDF framework to simulate flow in fractured porous media, where fractures are represented as highly permeable 1D features embedded within a 2D matrix *(Fig. 4a) (Koohbora., 2019)*. Henry's setup prescribes a constant freshwater flux on the inland boundary and hydrostatic seawater pressure on the seaside boundary, with no-flow conditions on the top and bottom boundaries. The Henry problem is governed by three key dimensionless parameters: the freshwater flux ratio (α), the Peclet number (β), and the domain aspect ratio (n) *(Abarca et al., 2007)*. Henry provided a semi-analytical solution for α = 0.263, β = 0.1, and n = 2.

$$a = \frac{q_b}{K_\epsilon} \quad b = \frac{D_m\phi}{q_b d} \quad \xi = \frac{L}{d} \quad (3)$$

The resulting solution shows a stable saltwater wedge beneath freshwater, shaped by the balance of advective and buoyancy forces *(Fig. 4b) (Abarca et al., 2007)*. Despite its conceptual clarity, discrepancies have arisen in reproducing the Henry problem due to variations in boundary condition interpretations, numerical approaches, and parameter values, particularly the diffusion coefficient (D) *(Abarca et al., 2007, Croucher and O'Sullivan, 2003,)*. Notably, Henry's original inland boundary condition, based on stream function gradients, is often approximated in modern codes by specifying either head or uniformly distributed inflow, though **neither exactly replicates field conditions**. Similarly, different forms of seaside boundary conditions, ranging from fixed concentrations to salt mass flux, have been proposed to better reflect real-world mixing behavior. The Henry problem remains a fundamental test case for validating numerical models of saltwater intrusion due to its semi-analytical solution and simplified, yet hydrologically insightful, formulation.

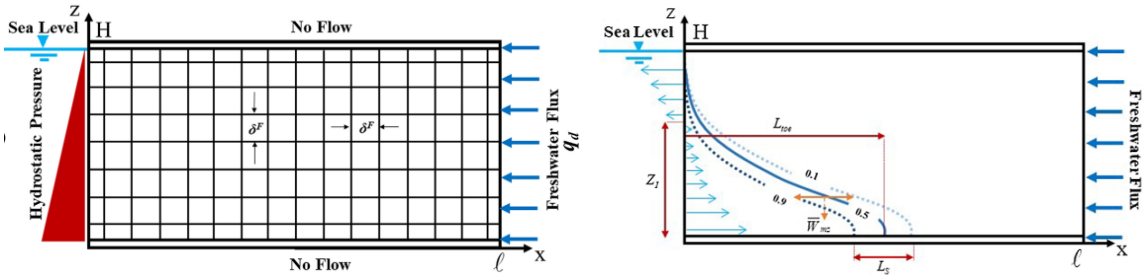

Fig. 4: (a)Conceptual model of the fractured Henry Problem with a network of orthogonal fractures configuration. (b) Schematic representation of the SWI metrics. (Koohbora., 2019).

What parameters control the position and geometry of the SWI?

In order to accurately simulate the saltwater wedge intrusion that forms at the interface between freshwater and seawater, it is essential to account for density differences and to incorporate the velocity field. This is typically done using a logarithmic scale to represent flow velocities, which allows the concentration to be shown in isolines rather than being omitted. *(Abarca et al., 2007, Lu & Werner, 2013)*. A primary metric is the **toe penetration**, defined as the horizontal distance from the seaside boundary to the point where the 50% isoconcentration line intersects the aquifer base, indicating the inland extent of saltwater intrusion *(Abarca et al., 2007)*.

Another key parameter is the **width of the mixing zone**, calculated as the vertical distance between the 25% and 75% isoconcentration lines, often averaged over a central segment of the wedge to minimize boundary effects *(Werner et al., 2013)*. While this width can be measured either vertically or perpendicularly to the interface, vertical measurement better reflects field observations *(Diersch & Kolditz, 2002)*. Both mean and variance of the interface profile provide insight into wedge dynamics. The nature of the mixing zone varies with the dominant transport process: **diffusion-dominated systems** exhibit broader, smoother transition zones, while **dispersion-dominated systems** display sharper, narrower wedges with steep salinity gradients *(Abarca et al., 2007, Voss & Souza, 1987)*.

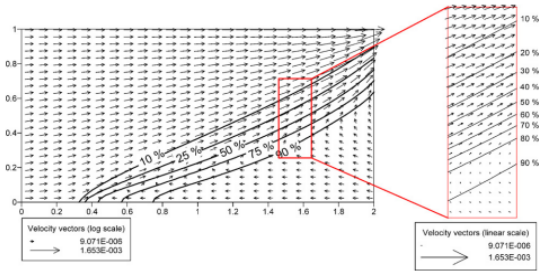

Fig. 10. Velocity field and 25, 50 and 75% concentration isolines in the dispersive reference case.

Fig. 5 . Velocity field using logarithmic scale to trace speed arrows at 25, 50 and 75% concentration isolines in the dispersive reference case. (Elena.A et al., 2006)

3. Geological context and hydrodynamics of the Roussillon basin

3.1 Geological context and geodynamic evolution of the region.

The plane of Roussillon is an extensive sedimentary basin, formed by the tectonic collapse during the Miocene, in the context of distension linked to the opening of the Mediterranean occidental basin, the Gulf of Lion. It is composed of the foreland basin associated with the collision between the Iberian plate and the Eurasian plate during the Eocene-Miocene, a major event that led to the resurrection of the Pyrenees. The basin then underwent extensive movements and thermal subsidence, processes that favor the accumulation of continental and marine sediments over several kilometers, starting from the Neogene up to the Quaternary period.

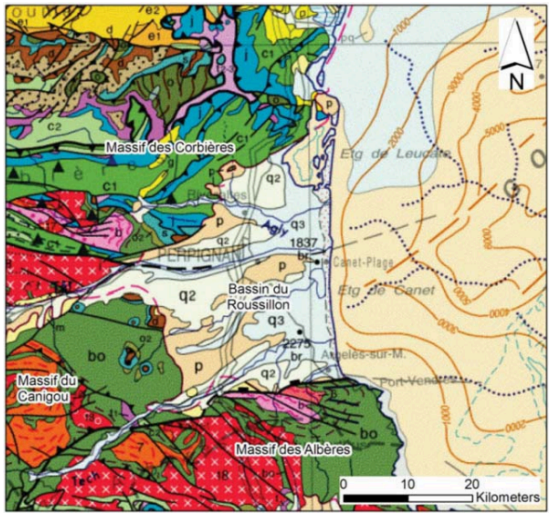

Fig. 6. Roussillon plain, BRGM, 2017.

The sedimentary filling of the Roussillon plain, composed of recent alluvial deposits carried by the neighboring rivers—Têt, Tech, and Agly—overlies older geological formations and illustrates the active interaction between fluvial and marine environments. This landscape continues to evolve today, influenced by residual tectonic activity and significant littoral dynamics due to the plain's proximity to the Mediterranean Sea. *(Caballero et al., 2020)*. Its basement is composed of ancient earth of Hercynian origin, primarily made up of metamorphic and granite rocks, noticeable today in the nearby massifs such as the Canigou and the Alberes. The geodynamic evolution that occurs post rift of the Gulf of Lion, combined with thermal subsidence and eustatic variations, plays a determining role in the current structure of the aquifer system. This has resulted in a heterogeneous filling of the basin, making hydrogeological modelling a complex feat, especially on what concerns the structure and the functioning of these aquifers.

3.2 Hydrogeological model and study well zone in the Roussillon plain.

Fig. 7. Delineation of the aquifers of the Roussillon Plain -Syndicat Mixte. *Fig. 8. Demmer 4 well. (Medjahed, 2024).*

Our study is focused on the Roussillon plain, which is bordered by several major mountain ranges: the Corbières, the Aspres, and the Alberes, as well as the valleys of the Agly, Têt, and Tech rivers.

The sediments that fill the plain were primarily deposited by the Agly, Têt, and Tech rivers, which drain the surrounding massifs. These massifs play an important hydrological role by recharging the aquifers with freshwater during periods of rainfall. A central focus of our study is the **Demmer 4 well**, located between Saint-Cyprien and Le Barcarès, which has yielded valuable data from previous projects. This well provides key insights into the structure and functioning of the coastal aquifers of the plain. It has supplied a range of hydrogeological and geophysical data, including measurements of hydraulic conductivity, piezometric levels, electrical fluid conductivity, salinity, gamma ray and resistivity logs, as well as lithological details from core samples and borehole stratigraphy.

4. Method

Water flow in CAs is a very complex process due to the mixing of two fluid phases (saltwater and freshwater) and resulting fluid density depends on the unknown salt concentration *(Voss & Souza, 1987)*. In this study, SWI in CAs was investigated through a combination of field measurements and numerical modeling.

4.1 Petrophysical Measurements and Geophysical Logging.

Petrophysical data obtained from borehole cores and geophysical well logs allows for the characterization of lithology and the estimation of hydraulic properties:

4.1.1 Permeability prediction models based on Nuclear Magnetic Resonance (NMR) logs:

NMR measurements provided estimates of porosity ϕ_{NMR} and permeability k_{NMR}, which are essential for understanding the flow capacity of the aquifer materials. Porosity and permeability can be estimated using empirical relationships derived from well log data and core sample analysis. Porosity was estimated from travel time using a least-squares regression approach, where a linear transform relates travel time to porosity *(Timur., 1968)*. Permeability was then estimated as a function of porosity, using a logarithmic transform fitted through regression analysis. The general form of the permeability-porosity relationship is commonly expressed as either

$$k = a\phi^{b} \text{ (Timur., 1968), or as } k = C\phi^{m}S_{win} \text{ (Coates et al., 1999)} \quad (4)\ (5)$$

Where k is permeability, ϕ is porosity, Swi is irreducible water saturation, and a, b, C, m, and n are empirical constants determined through calibration with core data.

These statistical methods are valid under the assumption that porosity and permeability are strongly correlated, but in cases of weak correlation, additional variables such as specific surface area or pore size may be needed to improve accuracy. The two models applicable in the permeability calculations are the kTIM, Timur-Coates (TIM) model *(Coates et al. 1999)*, which works in presence of hydrocarbons and kSDR, Schlumberger-Doll-Research (SDR) model *(Kenyon et al., 1997, 1988)*.

$$k_{TIM} = a.TPOR^{m}.\left(\frac{FEV}{BFV}\right) \quad \text{(Timur., 1968 et Coates et al., 1999)} \quad (6)$$

$$k_{SDR} = a.TPOR^{m}.(T_{2lm}))^{n} \quad \text{(Kenyon et al., 1997)} \quad (7)$$

Where k $[mD]$ *is the permeability;,* $TPOR$ [%] the *porosity;,* $T2lm$ $[ms]$ *the logarithmic mean of NMR T2 spectra;,*FEV [%], *Free Fluid Index;* BFV [%] , *Bulk Volume irreducible, m and n are the statistical model parameters, whose values can be derived from NMR experimental data sets of core samples.*

Data from the SWIMCLAS project, (*Medjahed., 2024)* using measurements from the Demmer 4 well, provides the basis for this graph. It illustrates two permeability profiles as a function of depth, with k_{SDR} shown in light blue and k_{TIM} in dark blue. Peaks represent zones of higher permeability, letting us observe sandy layers in contrast to clay.

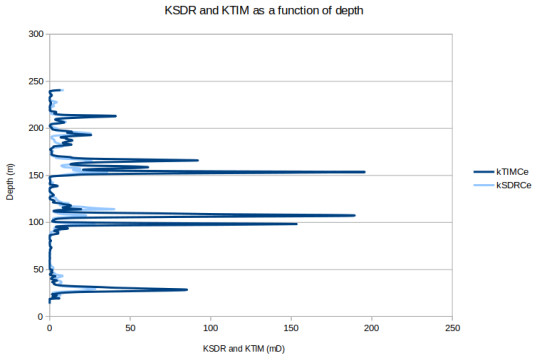

Fig. 9: k_{TIM} *and* k_{SDR} *as a function of depth.*

4.1.2 Hydraulic Conductivity:

Hydraulic conductivity is an essential parameter used in SWI simulation, its values are derived from core samples and cross-validated with NMR and logging data. The following formulas are used to calculate hydraulic conductivity:

$$K = \frac{k.\rho.g}{\mu} \tag{8}$$

Where k $[m^2]$ *is the permeability,* ρ $[kg/m^3]$ *density,* g $[m/s^2]$ *gravity acceleration with* $9.81\ m/s^2$, *and* μ $[kg/(m.s)]$ *dynamic viscosity.*

	Clay	Sand	Clay
kSDR [mD]	0,250116	274,48	0,172009
K [m/day]	2, 09 × 10−4	2, 03 × 10−1	1, 44 × 10−4

Table. 1. Hydraulic conductivity and permeability of the model layers.

The hydraulic conductivities can also be expressed in terms of intrinsic permeability k. In the following equation, k(z) is the intrinsic permeability. *(Dagan., 1996)*

$$K_f(z) = \frac{k\,(z)\,\rho_f}{\mu_f};\;\; K_s\,(z) = \;\; \frac{k\,(z)\,\rho_f}{\mu_s} \tag{9}$$

Where Kf(z) is the hydraulic conductivity for freshwater [m/s], Ks(z): Hydraulic conductivity for saltwater [m/s], k(z): Intrinsic permeability at depth z [m²], ρ the fluid density of freshwater and saltwater [kg/m³], g is the acceleration due to gravity [≈9.81 m/s²] and μ is the dynamic viscosity of the fluid.

4.1.3 Electrical conductivity of the pore fluid (Cw).

Bulk conductivity (C0) was obtained from the Demmer 4 through calculation using data from an electrical induction tool (EM51). The induction tool measures the bulk electrical conductivity (C0) values of the porous medium in-situ, which reflects the conductivity of both the rock matrix and the pore fluid. To isolate the pore fluid conductivity (Cw), the Waxman and Smits equation is used *(Waxman-Smits., 1968):*

$$C_0 = \left(\frac{C_w}{F}\right) + \;\; C_s \tag{10}$$

Where Cs is surface conductivity from clay minerals. F is a formation factor, related to porosity via Archie's Law (1942).

$$F = \;\; \emptyset^{-m} \tag{11}$$

ϕ *is the porosity estimated from Nuclear Magnetic Resonance (NMR) measurements.*
m, the cementation factor (connectivity index), typically between 1.5 and 2 for sandstones.

The pore fluid conductivity Cw is then computed as

$$C_w = (C_0 - \;\; C_s) \tag{12}$$

4.14 Surface Conductivity (Cs)

Surface conductivity is derived from the clay volume in the formation. For maximum surface conductivity Csmax, *Revill and Glover (1998)* propose:

$$C_{smax} = \left(\frac{2}{3}\right) pma.\;\beta_s.\;CEC_{max} \tag{13}$$

Where pma is a clay fraction, βs is a constant, CECmax is the maximum cation exchange quantity.

Ideally, C_s used to evaluate the model's sensitivity are determined from core measurements (CEC). Alternatively, C_s values can be chosen graphically based on the measured induction conductivity profiles opposite identified clay layers identified from gamma ray logs and core samples. The equations used to calculate this are as follows:

$$C_s = f\left(V_{shale}\right) \tag{14}$$

$$V_{shale} = \;\; \frac{GR - GR_{min}}{GR_{max} - GR_{min}} \tag{15}$$

Where V is volume, GR is gamma ray value at depth. GRmax, GRmin are the maximum/minimum gamma values used to estimate clay content.

4.2 Numerical modelling

Numerical simulations were used to model groundwater flow and SWI in the aquifer with the help of **MODFLOW** and **SEAWAT**, allowing them to simulate the dynamics and evolution of the saltwater wedge, variations in hydraulic head, and the effects of pumping and artificial recharge. The model incorporates the heterogeneous hydraulic properties from field data, VDF due to salt concentration gradients and boundary conditions representing freshwater recharge and seawater interface. In order to accurately conceive two-dimensional groundwater flow and transport models we use MT3D in our software to simulate this transport. The MT3DMS part of SEAWAT, referred to as the Integrated MT3DMS Transport (IMT) Process, solves the solute transport equation *(SEAWAT Version 4)*. It controls density dependent flow, which is crucial in the modelling of SWI while considering initial conditions, fluid viscosity and conduction at the boundaries. Groundwater flow equations used with VDF and solute transport are as follows:

$$\nabla.\left[\rho\frac{\mu_0}{\mu}K_0\left(\nabla h_0 + \frac{\rho-\rho_0}{\rho_0}\nabla z\right)\right] = \rho S_{s,0}\frac{\partial h0}{\partial t} + \theta\frac{\partial\rho}{\partial t}\frac{\partial C}{\partial t} - \rho_s q'_s, \tag{16}$$

Variable density groundwater flow (Langevin et al., 2008.).
Where $\rho 0$ *is the fluid density* $[ML-3]$ *at the reference concentration and reference temperature;* μ *is dynamic viscosity* $[ML-1T-1]$*; K0 is the hydraulic conductivity tensor of material saturated with the reference fluid* $[LT-1]$ *; h0 is the hydraulic head [L] measured in terms of the reference fluid of a specified concentration and temperature as the reference fluid is commonly freshwater. Ss, 0 is the specific storage* $[L-1]$*, defined as the volume of water released from storage per unit volume per unit decline of h0; t is time [T];* θ *is porosity [-]; C is salt concentration* $[ML-3]$*; and q is a source or sink [T - 1] of fluid with density* ρs.

The IMT Process solves for the following form of the solute transport equation:

$$\left(1 + \frac{\rho_b K_d^k}{\theta}\right)\frac{\partial(\theta C^k)}{\partial t} = \nabla.\left(\theta D.\nabla C^k\right) - \nabla.\left(qC^k\right) - q'_s C_s^k, \tag{17}$$

Transport equation (Langevin et al., 2008.).
ρb *is the bulk density mass of the solids divided by the total volume [ML - 3], Kd k is the distribution coefficient of species k L3M-1, Ck is the concentration of species k ML-3, D is the hydrodynamic dispersion coefficient tensor L2 T-1, q is specific discharge LT-1,and Cs k is the source or sink concentration ML-3 of species k.*

5. Results

This section presents the results obtained from the application of the methodology described above.

5.2 Data results.

Different models of conductivity (Cw) are generated using in-situ C0 profiles and assumed values of surface conductivity (Cs) from clay layers. Sensitivity analyses are conducted by varying **Cs,** which is based on varying clay content and **m** – the cementation factor (commonly tested between 1.5 and 2). These calculated Cw profiles, using EM51 tool data obtained from the well, allow direct comparison in different projects as references to one another. They may be compared against conductivity values obtained from average monitoring over intervals data from BRGM to interpret fluid distribution and behavior. This analysis helps assess the impact of surface conductivity and pore connectivity on Cw estimation.

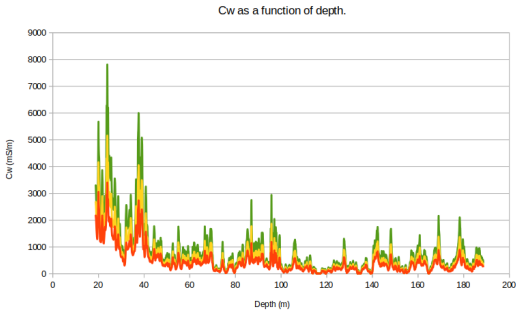

Fig. 10. Cw plot (Method 1)(Hamel., 2021)

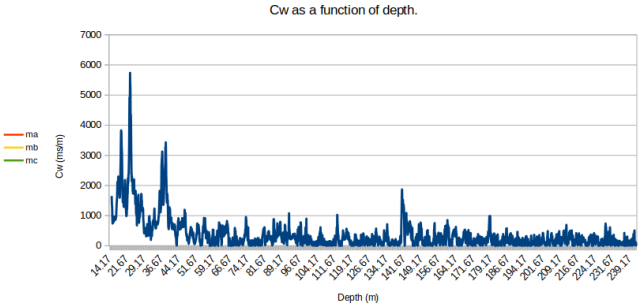

Fig. 11. Cw plot (Method 2)(Medjahed., 2024)

We therefore plot two sets of data from two different projects representing Cw values in the Demmer 4 well. Method 1 provides Cw values along the depth of the Demmer 4 well *(Fig. 10)*. In contrast, Method 2 explores the influence of different cementation factor values (m = 1.5, 1.75, and 2) to model Cw *(Fig. 10.)*, giving us three different curves. The method 1 graph displays a broader range and more pronounced trend compared to method 2. However, both profiles show a prominent peak around 25 meters of depth, followed by a similar downward trend till the bottom of the well. Overall, the results from both studies show a strong convergence in the interpretation of Cw variation along the well. The objective of this calculation is to create a reliable model of the subsurface pore fluid conductivity at a metric scale based on geophysical measurements. Gamma ray logs, used in parallel, help identify lithological changes—particularly the alternation between sandy and clayey layers—which supports the interpretation of the conductivity profiles by providing context about the sedimentary structure.

Cw values provide insight on the vertical and horizontal variations in conductivity, also indicating levels where saltier or more fresh water is flowing. We focus on the Method 2 values due to the single curve and elevated variations in conductivity, as well as results of up to almost 250 meters in depth. Cw along with values of permeability (k) (*Fig. 9*), helps infer both fluid type and the lithological context it moves through. When high Cw values align with high permeability (k), it suggests the presence of more saline water, often linked to specific lithological formations that allow greater flow. Conversely, low Cw associated with high permeability typically indicates fresh water circulation, reflecting more permeable and possibly coarser sediments. This combination (*Fig. 12*) helped SwimClas create parameters for the model we use today by combining k values with Cw values.

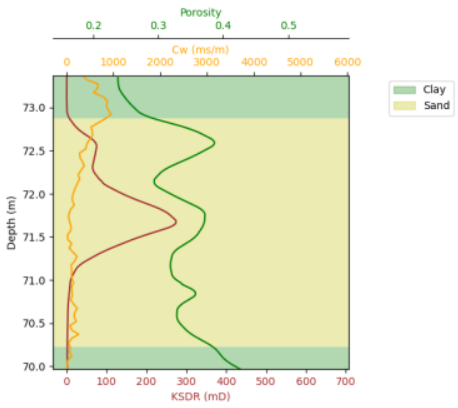

Fig 12: study interval model creation with Cw and k values. (Medjahed ., 2024).

5.3 Model results.

The model parameters include three alternating layers of clay and sand, each representing three different permeabilities *(Table. 2.)*.

Layers	Layer 1	Layer 2	Layer 3
Lithology	Clay	Sand	Clay
KSDR [mD]	0.250116	274.48	0.172009
Mean porosity [%]	0.40	0.34	0.25

Table. 2. Permeability and porosity of the model layers.

This modeling approach is similar to that used by *Mozafari et al. (2018)*, who also applied a variable-density flow framework to simulate SWI dynamics in CAs. The model grid is created through discretization (100 by 100 cells) and 100m by 250m in total dimension.

Layers	Layer 1 (m)	Layer 2 (m)	Layer 3 (m)
Top depth AQUIMER	69.97	80.22	152.84
Bottom depth AQUIMER	80.22	152.84	169.37
Width AQUIMER	250		

Table. 3.New model dimensions showing Top depth and Bottom depth of our study interval layers.

The initial conditions for the model are defined as follows: on the left boundary, a constant hydraulic head is imposed with a freshwater concentration set to c = 0. On the right boundary, the concentration is variable and corresponds to seawater, with c = 35 g/l. The top and bottom boundaries are assumed to be impermeable to solute transport, implying no-flow (zero-flux) conditions for both water and solutes. The groundwater flow is modeled using Darcy's law under VDF conditions, incorporating the effects of gravity and density dependence on salinity. Solute transport is governed by convection–diffusion processes, combining Fick's law (steady-state diffusion) for molecular diffusion and mechanical dispersion to represent the spreading of the saltwater–freshwater interface. For this study, the coefficient of diffusion (D) is an isotropic case, with a specific value of 0.57024 m2 /day.

Using our simulation software and previously existing SwimClas models, we calibrated the system by adjusting the **inflow rate qinflow** (m^3/day) and monitoring the resulting changes in **salt concentration** within the model. Initial simulations were performed using an inflow value of 600 m^3/day, consistent with the value provided by *(Caballero et al., 2022)*, and included adjacent clay layers to better reflect field conditions. These simulations provided insight into the fluxes, hydraulic head distribution, and salt concentration evolution across the model domain. We simulated qinflow at 400m^3/day and later at 100m^3/day, to reflect the natural variability of flow rates in the Roussillon aquifers.

In addition to our alternating layers *(Table. 3.)*, the model presents the variation and evolution of salt concentrations, from 0g/l to 35g/l. We visualize the Demmer 4- represented as a red dotted line. Our modifications aimed to produce more coherent salt concentration values near the well and to better represent the SWI geometry as a **wedge-shaped front**. The model we developed reveals a clear intrusion of saltwater from the left side of Demmer 4. *(Fig. 13.)*. In previous SwimClas models, we observed elevated hydraulic head values in the model, averaging around 40,000 meters for a qinflow of 600m³/day- an unrealistic result. In contrast, our model shows a more plausible hydraulic head of 13.4 meters at the same inflow rate. When qinflow is reduced to 400m³/day, the hydraulic head on the inland side of the model decreases further to approximately 8.9 meters *(Fig.14.)*. Model refinements allowed us to capture a more realistic evolution of salt concentration compared to previous versions. To enable this, we adjusted the spatial scale of the domain to focus on a smaller area, which enhanced detection of finer variations in system behavior. However, simulations with inflow rates below 400 m³/day exhibited limited salt concentration changes near the well, making it difficult to observe and analyse meaningful variations. *(Fig. 14, Fig.15.)*. This sensitivity to low inflow conditions poses a challenge for the applicability of our study.

ANR Aquimer (AQM) simulations with different qinflows.

AQM	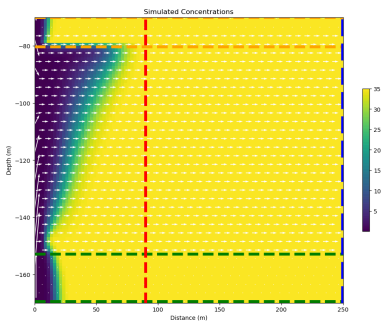	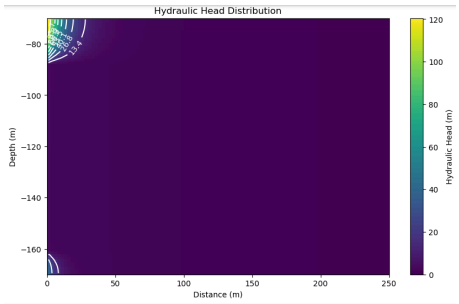
Q	600m³/day	

Fig.13 . Simulation conducted at 600m³/day.

	Qinflow (m³/day)	Hydraulic head
AQM	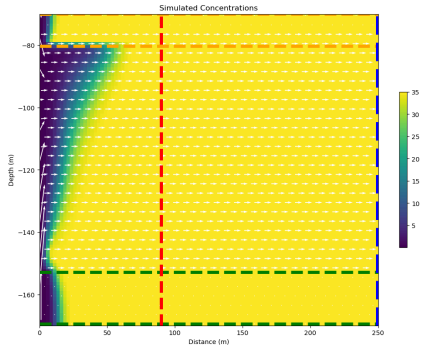	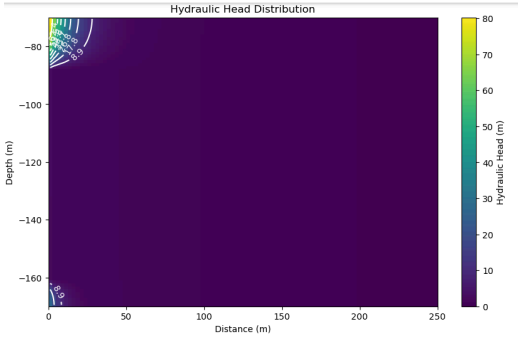
Q	400m³/day	

Fig.14. Simulation conducted at 400m³/day.

Variable densities along the well test.

Using piezometric data from the Demmer 4 well for the years 2021 - 2022 (*Brun., 2022*), along with the known densities of saltwater (~1025 kg/m³) and freshwater (1000 kg/m³), we applied the following formula in our model to simulate realistic pressure stratification scenarios.

$$h = \frac{P}{\rho g} + z \tag{18}$$

Where h is the total head (m), P is the pressure (Pa), ρ is fluid density (kg/m³), g is acceleration due to gravity (9.81 m/s²), and z the elevation of the point (m)(Cherry et al., 1979).

	Qinflow (m³/day)	Hydraulic head
AQM	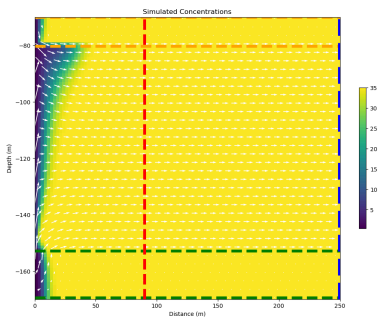	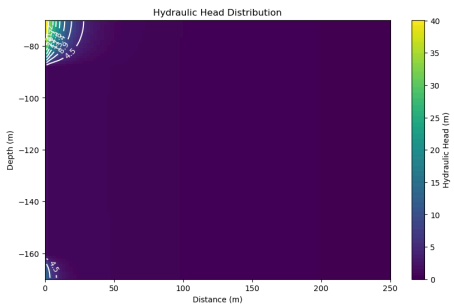
Q	100m³/day	

Fig.15 . Simulation conducted at 100m³/day.

This test aimed to replicate natural stratification, with denser saltwater accumulating at greater depths, and to assess whether pressure variations with depth influence the freshwater–saltwater interface. These results present a pinching effect on the SWI, consistent with our previous tests, and substantially lower influx of freshwater compared to our previous tests. We however still fail to portray accurate SWI geometry closer to the well and therefore merit revision.

These findings confirm the importance of pressure distributions within the well and aquifers in controlling the interface behaviour and the dynamics of fluid flow.

6. Discussion

The results of this study underscore several important insights into the mechanisms governing SWI in CAs. Chief among these is the critical influence of vertical permeability contrasts on the behavior and stability of the saline front. These vertical contrasts significantly control the vertical and lateral movement of saline water, often resulting in complex interface geometries. They act as accelerators for salinity migration depending on permeability and porosity, and may determine the effectiveness of aquifer recovery during recharge phases. While previous models provide a general understanding of SWI under similar lithological configurations (*Mozafari., 2018* , *Khoobora ., 2019*), our model offers finer scale resolution in salt front dynamics due to its incorporation of heterogeneous layering and realistic inflow variability.

Natural recharge zones, such as the Corbières Massif, also play a pivotal role in counteracting saltwater encroachment by delivering fresh groundwater during recharge periods, thereby influencing the inland extent and saline wedge dynamics*(Caballero et al.,2021)*. However, interpretation of results should consider key uncertainties. For instance, the hydraulic head imposed on the seaward boundary, currently set to zero, may not reflect actual conditions and warrants revision. Additionally, the dominant flow direction remains uncertain, whether inland to seaward, from east to west, or in the reversed direction due to anthropogenic pumping, which has direct implications for intrusion modeling. The Demmer 4 well is particularly notable for its slightly elevated piezometric head compared to surrounding wells, hinting at localized hydrogeological features *(Hamel., 2021)*. Lastly, Nuclear Magnetic Resonance (NMR) has demonstrated promise for characterizing transport parameters in heterogeneous sediment media, however further calibration of hydraulic heads and consistency between imposed flow rates and the model scale used are essential for improving simulation fidelity. We need improved representation of salt concentration near wells—especially under low inflow scenarios—because reduced freshwater input diminishes the system's ability to simulate saline intrusion, particularly in zones of higher permeability.

7. Limitations and perspectives

A primary limitation of the current model concerns the classical Henry problem, it exhibits well-known limitations, including its inability to replicate observed salinity profiles (it can only approximate) and its sensitivity to diffusion parameters and boundary conditions *(Abarca et al., 2007, Croucher and O'Sullivan, 2003)*. Specifically, the Henry problem tends to overestimate mixing due to a high diffusion coefficient (D) and fixed concentration at the seawater boundary, resulting in a smoother, less realistic salt front. Secondly, in our current model, the low freshwater inflow rate (qinflow) prevents the development of meaningful salt concentration gradients *(Fig. 14. and Fig. 15.)*, limiting our ability to observe and interpret the dynamics of saltwater intrusion under varying recharge conditions. Although significant progress has been made, several open questions remain: *What specific modifications (e.g., boundary condition formulations, parameter calibrations) are most effective for improving saltwater intrusion modeling in Roussillon's CAs? To what extent do different domain scales and hydrogeological heterogeneity (e.g., sediment layering) influence the model outcomes?* To better understand the system's response, future modeling should focus on systematic sensitivity analyses, testing parameters both individually and in coupled configurations to identify dominant controls and interactions. Additionally, tests of modelling without alternating clay layers should be conducted firstly, and then later incorporated back into the model to better comprehend a one-layer model type intrusion. Lastly, more advanced dispersive models should be explored- specifically those that incorporate velocity-dependent dispersion and anisotropic hydraulic conductivity- in order to accurately yield a more physically realistic representation of both flow and solute transport processes in model systems, and to broaden its applicability to varied hydrogeological contexts. *(Dentz et al., 2004, Koohbora, 2019)*.

8. Conclusion

This study advances the understanding of saltwater intrusion (SWI) dynamics in coastal aquifers by integrating conductivity modeling, petrophysical data, and numerical simulation under variable-density flow conditions. The observed relationship between pore fluid conductivity (Cw) and permeability (k) (Fig. 10, Fig. 11), enables a more nuanced interpretation of lithology–fluid interactions, while simulation outcomes underscore the critical influence of **vertical heterogeneity** and **inflow variability** on SWI behavior. The study emphasizes the importance of incorporating depth-dependent permeability to realistically simulate the wedge-shaped intrusion driven by density contrasts between freshwater and seawater. We investigated the implications of recharge dynamics

and highlighted the need for more advanced dispersion models to improve the accuracy of SWI simulations. The refined model captures more realistic spatial variations in salt concentration, particularly under fluctuating freshwater inflow scenarios. While substantial progress has been made, further work is required to refine boundary condition formulations, enhance aquifer characterization, and improve model calibration. These steps are essential to strengthen the predictive capacity of SWI models and inform sustainable groundwater management in diverse coastal hydrogeological contexts.

9. Remerciements

I would like to sincerely thank Madame Delphine Roubinet, Research Director at CNRS and the Géosciences Montpellier laboratory, for accepting my internship request, for her patience, valuable advice, and guidance throughout this internship.
I am grateful to Laurent Brun for his warm welcome and support during the internship.
Thanks also to Madame Johanna Lofi, PhD in Marine Geology and Sedimentary Geophysics, for her helpful advice.
Finally, I would like to acknowledge all those who actively contributed to the data acquisition during this internship: Monsieur Philippe Pézard, Yohann Cousquer, Célina Medjahed, and Simone Barry.

10. References

Dall'Alba, Valentin & Renard, Philippe & Straubhaar, Julien & Issautier, Benoît & Duvail, Cédric & Caballero, Yvan. (2020). 3D Multiple-point Statistics Simulations of the Roussillon Continental Pliocene Aquifer using DeeSse. 10.5194/hess-2020-96.

Behshad Koohbora, Marwan Fahsa, , Behzad Ataie-Ashtianib,c, Benjamin Belforta, Craig T. Simmonsc, Anis Younes. (2019). Uncertainty analysis for seawater intrusion in fractured coastal aquifers: Effects of fracture location, aperture, density and hydrodynamic parameters

SRUTHI S KUMAR, S DEB BARMA and MAHESHA AMAI. (2020). Simulation of coastal aquifer using mSim toolbox and COMSOL multiphysics.

Coates, G., Xiao, L., & Prammer, M. G. (1999). NMR logging: Principles and applications. Halliburton Energy Services.

Mozafari, M. (2018). Coupled modeling of variable-density flow and solute transport in coastal aquifers: Implications for saltwater intrusion. Journal of Hydrology, ***563****, 113–125. https://doi.org/10.1016/j.jhydrol.2018.05.028*

Anatoly Legchenko , Jean-Michel Baltassat, Alain Beauce, Jean Bernard (2002).Nuclear magnetic resonance as a geophysical tool for hydrogeologists.

A.A. Portselan, V.V. Treshchenkov (2002). Application of the NMR-tomography technique for groundwater investigations in Equatorial Africa: a case-history in Guinea.

A. Guillen, A. Legchenko (2002). Inversion of surface nuclear magnetic resonance data by an adapted Monte Carlo method applied to water resource characterization.

Ugur Yaramanci, Gerhard Lange , Marian Hertrich (2002). Aquifer characterisation using Surface NMR jointly with other geophysical techniques at the Nauen/Berlin test site.

Marian Hertrich, Ugur Yaramanci (2002). Joint inversion of Surface Nuclear Magnetic Resonance and Vertical Electrical Sounding.

M.D. Schirov , A.D. Rojkowski (2002). On the accuracy of parameters determination from SNMR measurements.

O. Mohnke, U. Yaramanci (2002). Smooth and block inversion of surface NMR amplitudes and decay times using simulated annealing.

Werner, A. D., Simmons, C. T., Lu, C., & Abarca, E. (2013). Quantifying uncertainty in saltwater intrusion metrics through Monte Carlo analysis of variable-density flow.

Timur, A. (1968) An Investigation of Permeability, Porosity, and Residual Water Saturation Relationships for Sandstone Reservoirs. Society of Petrophysics and Well-Log Analysts.

Dagan, G., & Zeitoun, D. G. (1998). Seawater–freshwater interface in a stratified aquifer of random permeability distribution. Journal of Contaminant Hydrology, 29(3), 185–203. https://doi.org/10.1016/S0169-7722(97)00013-2

R. Supper, B. Jochum, G. Hübl, A. Römer, R. Arndt (2002). SNMR test measurements in Austria.

Max A. Meju, Paul Denton, Peter Fenning (2002). Surface NMR sounding and inversion to detect groundwater in key aquifers in England: comparisons with VES–TEM methods.

Peter B. Weichman, Dong Rong Lun, Michael H. Ritzwoller, Eugene M. Lavely (2002). Study of surface nuclear magnetic resonance inverse problems.

Langevin, C. D., Thorne Jr., D. T., Dausman, A. M., Sukop, M. C., & Guo, W. (2008). SEAWAT Version 4: A computer program for simulation of multi-species solute and heat transport (Techniques and Methods 6-A22). U.S. Geological Survey. https://doi.org/10.3133/tm6A22

Abarca, E., Carrera, J., Sánchez-Vila, X., & Dentz, M. (2007). An overview of the Henry problem. Advances in Water Resources, 30(5), 913–926. https://doi.org/10.1016/j.advwatres.2006.08.005

Croucher, A. E., & O'Sullivan, M. J. (2003). The Henry problem for saltwater intrusion. Water Resources Research, 39(1), 1–7. https://doi.org/10.1029/2001WR000633

Dentz, M., Tartakovsky, D. M., & Abarca, E. (2004). Perturbation approach to the Henry problem. Water Resources Research, 40(4), W04201. https://doi.org/10.1029/2003WR002850

Diersch, H.-J. G., & Kolditz, O. (2002). Variable-density flow and transport in porous media: Approaches and challenges. Advances in Water Resources, 25(8–12), 899–944. https://doi.org/10.1016/S0309-1708(02)00063-5

Voss, C. I., & Souza, W. R. (1987). Variable-density flow and solute transport simulation of regional aquifers containing a narrow freshwater–saltwater transition zone. Water Resources Research, 23(10), 1851–1866. https://doi.org/10.1029/WR023i010p01851

Kenyon, W. E. (1997). Petrophysical principles and applications of NMR logging. The Log Analyst, 38(2), 21–43.

Bear, J. (1972). Dynamics of Fluids in Porous Media. Dover Publications.

11. Annexes

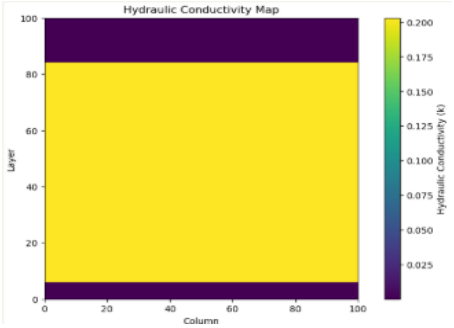

Annexe 1. Hydraulic conductivity map of our model showing alternating layers.

	Qinflow (m³/day)	Hydraulic head
	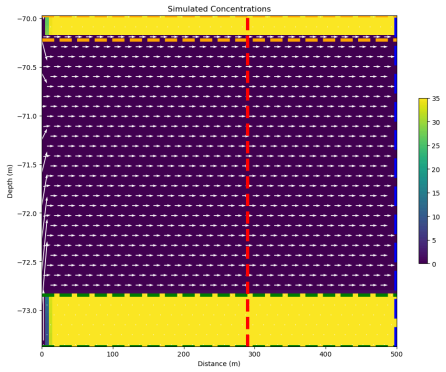	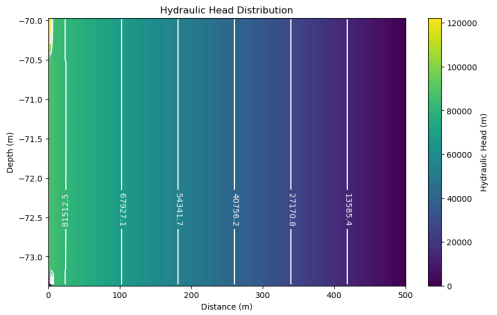

Annexe 2. Initial SWIMCLASS model (3m by 500m) at qinflow 600m³/day*(Medjahed., 2024)*.

	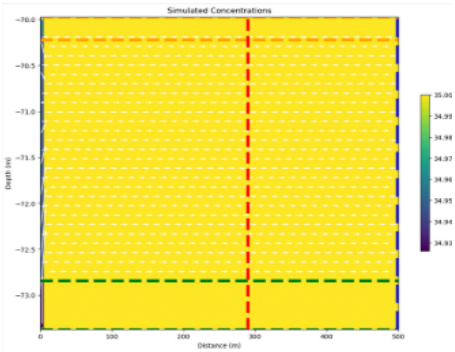	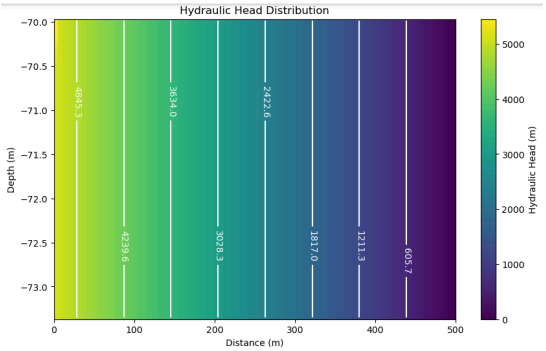
Q	5.7 m³/day (Initial SwimClas model)	

Annexe 3. Initial SWIMCLASS model (3m by 500m) at qinflow 5.7m³//day*(Medjahed., 2024)*.

Calendar of task distribution during the internship.